# Phase and group velocity measurements from physically modeled transmission gathers

Faranak Mahmoudian, Gary Margrave, and Joe Wong

## ABSTRACT

Physical model data have been used for many years to simulate exploration targets, as in the example of a fractured medium. Yet, physical modeling is challenging for at least two reasons, (1) the initial characterization of the medium is difficult, and (2) the large highly-directional transducers used as sources and receivers cause distortions. The initial characterization of a laboratory physical model is done by determination of elastic stiffness coefficients from the phase or group velocity measurements along various directions. We present a review on how to measure phase and group velocities from physical model transmission gathers acquired using piezoelectric transducers with different sizes. Group velocity measurements are found to be straightforward, reasonably accurate, and independent of the size of the transducers used. In contrast, the accuracy of phase velocities derived from the $(\tau, p)$ transform analysis was found to be very sensitive to small differences in picked arrival times and to transducer size. Compared to the phase-velocity procedure, the technique involving group velocities is much less prone to error due to time-picking uncertainties, and therefore is more suitable for analyzing physical model seismic data.

## INTRODUCTION

In physical seismic modeling, an alternative to numerical modeling, the seismic data are acquired over small, laboratory sized geological models. Physical modeling has been used to evaluate the accuracy of mathematical models of wave propagation, to test seismic data processing algorithms, and to provide insights into the interpretation of 3C seismic data acquired over complex media (Ebrom and McDonald, 1994). Further, it has acquired relevance as a method for studying anisotropic media, because waves in laboratory scale models obey the same physical laws as waves propagating in the anisotropic earth. In physical modeling of anisotropic media, fractured media in particular, the first matter to be addressed is the construction of a model that is reasonably representative of a geological feature, with known anisotropic elastic properties. Knowing the $6 \times 6$ stiffness coefficient matrix and density of the laboratory model determines all its elastic properties.

The stiffness coefficients can be estimated from phase or group velocities of the three quasi-body wave types; a quasi-compressional (qP) and two quasi-shear (qS) modes. There are well-known exact explicit relations between the anisotropic stiffness coefficients, in particular for orthorhombic symmetry, and the quasi-body wave's phase velocities, obtained from the solution of the Christoffel equation (Musgrave, 1970; Tsvankin, 1997). Consequently, the anisotropic stiffness coefficients are most often determined by measuring phase velocities (e.g., McSkimin, 1967; Vestrum et al., 1999; Mah and Schmitt, 2001). The phase velocity approach leaves no doubt as to which of the stiffness coefficients can be recovered, and the uncertainties in the value of stiffness coefficients can usually be related in a simple way to the experimental errors in the phase velocity measurements. For large physical models, however, measurements of phase velocities are problematic, require special ex-

perimental setups if the $(\tau, p)$ transform method is employed, dependent upon the size of transducers used, and prone to large errors. A straightforward alternative to phase velocity methods is employing the group velocity which controls the traveltime and is easy to measure and less prone to errors. For group velocity, exact explicit relationships to the stiffness coefficients are not well-known, which can be manipulated to obtain the stiffness coefficients directly. The existing methods for recovering stiffness coefficients from group velocities employ indirect procedures to obtain the stiffness coefficients from group velocity measurements, for more explanation see Mahmoudian et al. (2013).

In this report, using numerical simulation, the methods for measuring both phase and group velocities from physical modeling transmission gathers are explained and compared. The group velocity measurements are found to be straightforward, reasonably accurate, and independent of the size of the transducers used. In contrast, the phase velocity measurements require specialized acquisition geometries, are prone to large measurement errors, and are quite sensitive to the size of the transducers used. Over an anisotropic model, we measured the phase and group velocities along various directions from physical model transmission gathers. The group velocity measurements were then used to estimate the density-normalized stiffness coefficients of the phenolic model which is presented elsewhere Mahmoudian et al. (2013). The group velocity measurement from physical model data is straightforward, accurate, independent of the size of the transducers used (hence practical), and is particularly useful for initial characterization of an orthorhombic physical layer, required in advance of using the layer in any physical modeling seismic survey.

## BACKGROUND

Seismic anisotropy is the dependence of elastic wave velocities through a medium on the direction in which the elastic wave is traveling. The phase velocity is the wavefront's propagation velocity in the direction normal to the wavefront, and the group (ray) velocity is the energy propagation velocity. Consider the reference Cartesian coordinate system, $(x_1, x_2, x_3)$, associated with the three orthorhombic symmetry planes. Along the coordinate principal directions (i.e. $x_1$-, $x_2$-, and $x_3$-axes), phase and group velocities are equal. In this reference coordinate system, the nine independent orthorhombic density-normalized stiffness coefficients are the six diagonal $A_{ii}$ plus three off-diagonal terms ($A_{23}, A_{13}, A_{12}$). The quasi-body wave velocities along the coordinate principal axes determine diagonal stiffness coefficients (Table 1), the $A_{ii}(i = 1 : 3)$ from the three quasi-P (qP) velocities, and the $A_{ii}(i = 4 : 6)$ from the three quasi-S (qS) velocities. The off-diagonal stiffness coefficients, however, are not individually related to the phase or group velocity along some particular directions. Determination of the off-diagonal density-normalized stiffness coefficients from group velocity measurements are explained in Mahmoudian et al. (2013).

## VELOCITY MEASUREMENTS

For rock samples, seismic velocities are often measured using relatively large ultrasonic transducers in a transmission geometry (Bouzidi and Schmitt, 2009). Using two flat-faced transducers attached to the model in various propagation directions, body-wave velocities can be measured by picking arrival times. According to Dellinger and Vernik (1994) and

| Polarization | Propagation | | |
|---|---|---|---|
| | $x_1$ | $x_2$ | $x_3$ |
| $x_1$ | $V_{11} = \sqrt{A_{11}}$ | $V_{12} = \sqrt{A_{66}}$ | $V_{13} = \sqrt{A_{55}}$ |
| $x_2$ | $V_{21} = \sqrt{A_{66}}$ | $V_{22} = \sqrt{A_{22}}$ | $V_{23} = \sqrt{A_{44}}$ |
| $x_3$ | $V_{31} = \sqrt{A_{55}}$ | $V_{32} = \sqrt{A_{44}}$ | $V_{33} = \sqrt{A_{33}}$ |

Table 1. Body waves' velocities along the principal axes. Here $V_{ij}$ $(i, j = 1, 2, 3)$ is the body wave velocity which propagates along the $x_j$-axis and is polarized along the $x_i$-axis. For example $V_{11}$ is the qP velocity propagating along the $x_1$-axis, and $V_{23}(= V_{32})$ is the qS velocity propagating along the $x_3$-axis and polarized along the $x_2$-axis.

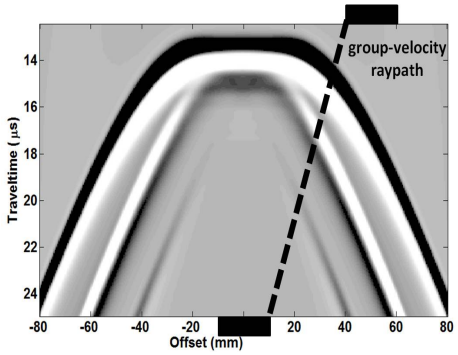


FIG. 1. A transmission gather using large transducers, modeled by an acoustic finite-difference method, over a model with the size of $160 \times 80$mm$^2$. The black parallel vectors show the travel path of the plane-wave portion of the wavefront. The transducer's size is chosen to be half of the layer thickness to exaggerate the plane-wave generation.

Vestrum (1994) such measurements estimate group velocities if the source-receiver separation is large compared to the transducer dimension. If the transducers are large compared to their separation, they will approximately transmit and receive plane waves over a large spatial interval (Figure 1), thus enabling direct phase velocity measurement. For a small specimen to measure phase velocity using large transducers, the specimen is cut appropriately along various directions to make the desired contact plane for the flat-faced large transducers. The phase velocity along the direction normal to the cut planes then can be measured. Next, we describe measuring group and phase velocity on large physical models which simulate some geological features rather than on small core samples.

## NUMERICAL SIMULATIONS

### Group velocity

Consider a physical model transmission gather, where the source transducer is located on one side of the model and the receiver profile is positioned on the other side. Treating the physical model as a homogeneous plane layer, for small transducers which approximate point sources and receivers, the length of the straight line connecting the centers of the transducers divided by the first arrival traveltimes yields a good estimate of the group velocity in the source-receiver center-to-center raypath direction. For large source and receiver transducers, the effective source-receiver raypath is the straight line connecting the nearest-edges of source and receiver transducers, because the energy propagates the minimum distance between the transducers. Brown et al. (1991) calculated the group velocities in various directions by dividing such effective source-receiver raypaths by the first arrival

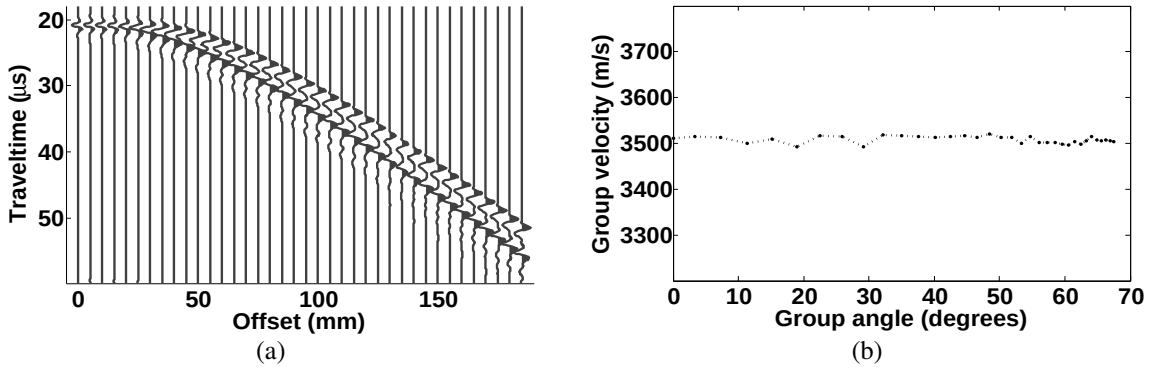


FIG. 2. (a) Finite-difference generated transmission gather over a constant velocity layer with a velocity of $3500$m/s and thickness of $70$mm and source and receiver size of $13$mm. This is an $2$D acoustic wave propagating through a uniform velocity grid with the grid size of $0.5$mm and time step of $0.05\mu$s. (b) Measured group velocity.

traveltimes of each mode. We follow their method in measuring the group velocities. Hence the effective size of transducers needs to be known. The effective size of a transducer is defined by the active portion of the piezoelectric crystal, and may be slightly different from the nominal dimension given by the manufacturer. The appropriate effective transducer size is determined from preliminary measurements in an isotropic homogeneous plexiglas layer. The justification for considering the nearest-edges distance as the raypath taken by the first arrival energy is provided below.

We assume that a circular physical model transducer can be considered to be a continuous seismic source/receiver array. Considering a source transducer, assuming Huygens's principle, a transducer can be regarded as circular array of point sources where each individual element radiates the same waveform simultaneously with the others. Using acoustic finite-difference modeling over a $70$mm isotropic layer with a constant velocity of $3500$m/s, we generated a transmission gather utilizing linear* source and receiver arrays representing a transducer with the diameter of $13$mm (Figure 2a). The finite-difference program we used, utilizes a second-order nine-point approximation to the Laplacian operator†. The time steps were chosen to be small enough to ensure that grid dispersion is as small as numerically possible. A minimum phase wavelet with a dominant frequency of $500$kHZ was used as the initial wavelet. In the finite-difference generated transmission gather (Figure 2a), the change in wavelet shape from near to far offsets is apparent and is due to the finite sizes of source and receivers. The $13$mm source/receiver is implemented using source/receiver array, with the array length of $13$mm. The wavelet change is due to the array effect. Figure 2b shows the measured group velocity, obtained from first arrival times divided by the nearest-edges distance between transducers, versus the group angle with the error of $\pm 10$m/s.

Using the edge-to-edge distance rather than the center-to-center distance between the source and receiver transducers, is a simple geometrical correction. Figure 3 shows the

*In a linear array, every point has the same weight.
†Software from CREWES MatLab library.

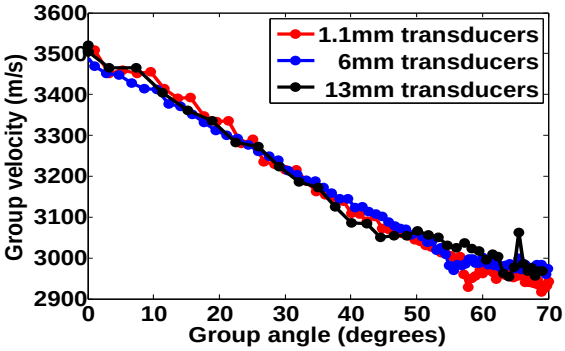


FIG. 3. Group velocity estimated from transmission data, $(x_1, x_3)$ plane, acquired with three transducer sizes using the edge-to-edge distance correction.

group velocities of the experimental phenolic layer measured from physical model transmission gathers acquired with $1.1$mm, $6$mm, and $13$mm transducers after the edge-to-edge correction. The measurements from these three transducer sizes are consistent to within the picking error, and independent of the size of the transducer used.

## Phase velocity

Kebaili and Schmitt (1997) presented a method using the $(\tau, p)$ transform to measure phase velocity from two transmission shot gathers with two different shot depths. Consider two transmission shot gathers recorded with the shots at depths of $d_1$ and $d_2$, acquired by point sources and receivers (Figure 4a). In each transmission gather the first arrival event of each mode, for example P-wave, appears as a hyperbolic event (Figure 4b). Taking the $(\tau, p)$ transform, the first arrival hyperbola will be mapped to an apparent ellipse[‡] (Figure 4c). In each transmission gather, consider the line with the slope of $p_0$ ($t = \tau_1 + p_0 x$ and $t = \tau_2 + p_0 x$) tangent to the first arrival hyperbola (Figure 4b). These lines designate plane waves traveling with the horizontal slowness of $p_0$, intercepting the time axis at $\tau_1$ and $\tau_2$. Summation along these two lines produces the two points, $(\tau_1, p_0)$ and $(\tau_2, p_0)$, on each $(\tau, p)$ event, respectively. Effectively, the $p_0$ plane wave has traveled the vertical distance of $d_2 - d_1$ with the vertical slowness of $q_0 = (\tau_2 - \tau_1)/(d_2 - d_1)$ from the source at $d_1$ to the source at $d_2$. Therefore, for any particular horizontal slowness of $p_0$ in the $(\tau, p)$ domain, the two $(\tau_1, p_0)$ and $(\tau_2, p_0)$ points, picked from the transform of the first arrival hyperbolic events, will estimate the phase velocity as $v_{p_0} = ({p_0}^2 + {q_0}^2)^{(-1/2)}$.

For a point source and receivers, we generated two finite-difference transmission gathers through an isotropic layer with the constant velocity of $3500$m/s, with the shot depths at $d_1 = 40mm$ and $d_2 = 50mm$ (Figure 5). For each $p_0$, the corresponding $(\tau_1, p_0)$ and $(\tau_2, p_0)$, are picked from the ellipses in the $(\tau, p)$ transforms of the two gathers. Figure 6a shows the measured phase velocities versus phase angle. As is apparent, the Kebaili and Schmitt (1997) method successfully measures the constant phase velocity of $3500$m/s with an error of $\pm 50$m/s due to picking uncertainty. Assuming a point source and a sufficient number of point receivers, the picking in the $(\tau, p)$ transform can be done consistently on

[‡]Note, pure hyperbola and ellipse events are only true for isotropic case.

first arrival, peak, or trough within this error range.

Next, we repeated the same finite-difference transmission gathers, using source and receivers with the simulated size of 13mm. The receivers were attached to the top surface (Figure 4a), and the source transducer at the side of the layer with its top edge at the depths of $d_1$ and $d_2$. Figure 6b shows the measured phase velocity comparing the results when it was picked on the first arrival, peak or trough (Figure 5b). The measured phase velocity has the error range of $\pm 400$m/s when peak or trough was picked (Figure 6b), but seems more accurate with error range of $\pm 150$m/s when first arrival was used. We believe that such large errors are related to the loss of resolution caused by the finite-size sources and receivers, which was simulated by using source/receiver arrays. Essentially, the array effect is a spatial averaging and the resulting distortion is less for first arrivals than for subsequent arrivals. For physical model data acquired over anisotropic models, this wave interference plus the presence of noise in the data reduces the reliability of phase velocity measurements. Hence, for phase velocity measurements smaller transducers, resembling point sources and receivers, as used in Mah and Schmitt (2001), are desired. This contrasts with the results in the previous section where we showed that the measurement of group velocity is less sensitive to transducer size.

## PHYSICAL MODEL EXPERIMENT

Our physical modeling system has a scale of $(1 : 10000)$ for both length and time. This means that, for example, 1mm in the physical model represents 10m and a frequency of 500kHz represents a frequency of 50Hz in the real earth. Having the same scale for length and time allows the velocity of the medium to remain unscaled. We used flat-faced circular piezoelectric transducers of three different for acquiring transmission data. These compressional and shear-wave (P and S) transducers convert electrical energy to mechanical energy and vice-versa, thus being capable of acting as either sources or receivers. As a receiver, the P- and S-transducers are sensitive to displacement normal and tangential to the contact face of the transducer, respectively, and represent vertical and horizontal component geophones. As a source, either P- or S-transducers generate both P- and S-waves, but generally stronger P-wave emanates from the P-transducer and stronger S-waves emanate from the S-transducer. We took special measures in coupling S-transducers to a solid surface to decrease the P-wave amplitudes produced by S-transducers.

Our modeling system is equipped with a robotic positioning system which has a positioning error less than 0.1mm. There are separate arms for both the source and receiver. Trace stacking of repeated source excitations for each receiver position and the progressive re-positioning of the receiver transducer generates a seismic gather. The location of a transducer is assigned to the location of the center of its contact face. We manually position the first source and receiver locations according to a predefined coordinate system. Once the initial source-receiver offset is set, the subsequent increments in offset are computer controlled, and as a consequence are accurately known. The source pulse is highly repeatable over many hours of acquisition. More details about the laboratory equipment and set-up are described in Wong et al. (2009).

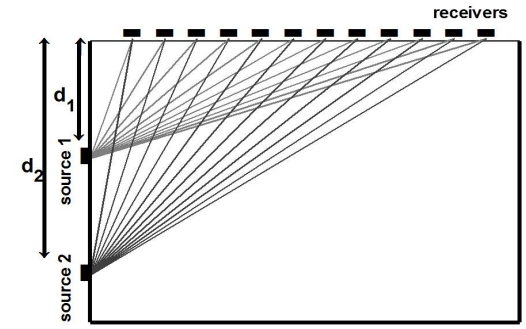


(a)

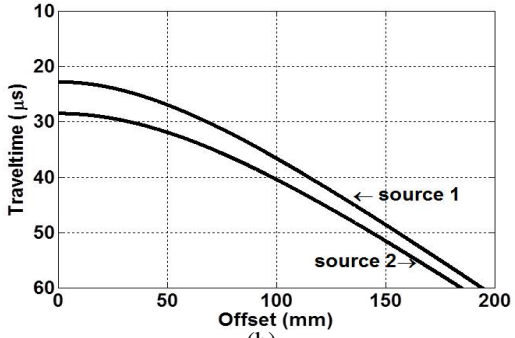


(b)

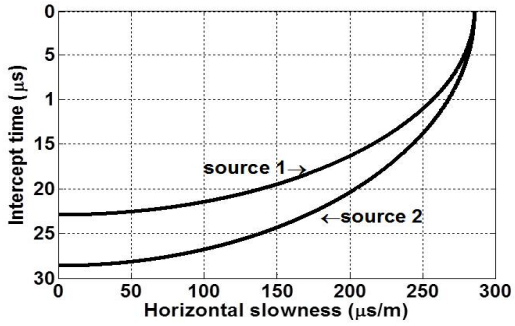


(c)

FIG. 4. (a) Schematic view of the acquisition geometry of the two transmission gathers required for measuring the phase velocity. (b) The two traveltime versus offset curves for the two transmission gathers with different source positions. (c) $(\tau, p)$ transforms of the traveltime curves in (b). Note the determination of $\Delta\tau = \tau_2 - \tau_1$ at a given horizontal slowness $p_0$ (Mah and Schmitt, 2001).

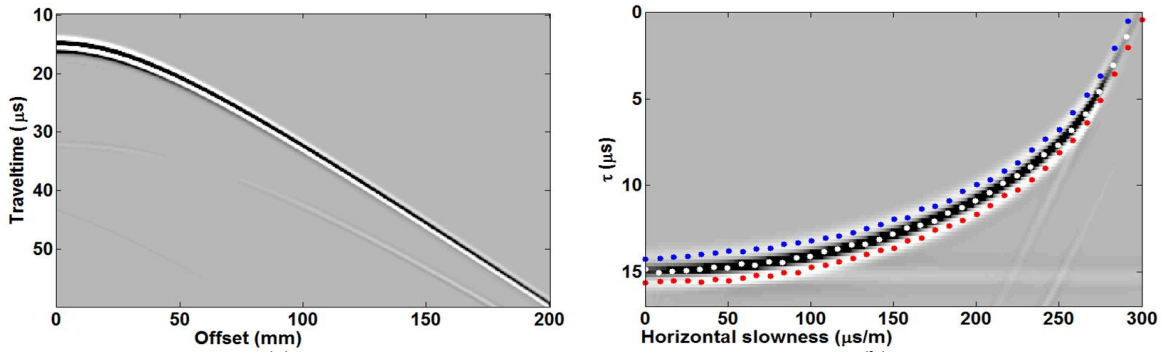


(a) (b)

FIG. 5. (a) Finite-difference generated transmission gather assuming point source and receivers, with the shot depths at $d_2 = 50mm$, over a constant velocity layer with the velocity of $3500$m/s. (b) The $(\tau, p)$ transform of the gather in (a). The first breaks picks are shown by blue dots, on peaks are shown by white dots, and on trough are shown by red dots. Two of such transmission gathers, with the shot depths at $d_1 = 40mm$ and $d_2 = 50mm$, were used in the estimation of phase velocities.

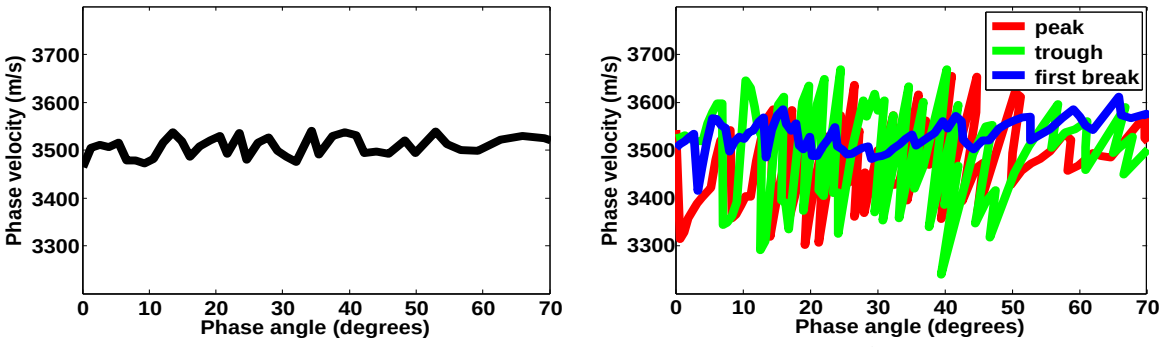


(a) (b)

FIG. 6. Phase velocity measured from finite-difference data gathered over an isotropic layer with the constant velocity of $3500$m/s. (a) Point source and receiver data. (b) $13$mm transducer data.

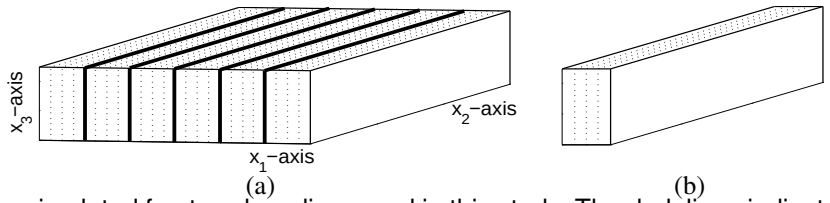


FIG. 7. (a) The simulated fractured medium used in this study. The dark lines indicate glued seams between separate phenolic blocks. (b) A slab of phenolic material with the dashed lines displaying the linen planes.

### Simulated fractured layer

We constructed a simulated fractured medium from phenolic LE-grade material, at the University of Calgary, CREWES Project. Phenolic LE is composed of laminated sheets of linen fabric bonded together with phenolic resin, and has mass density of $1390$ kg/m$^3$. To construct our simulated fractured layer, the original board of phenolic material with horizontally-laid linen fabric was cut into slabs along planes orthogonal to the plane of linen layers. These were rotated $90^\circ$ and bonded together under a uniform high pressure with epoxy. This constructed layer simulates a VTI medium with vertical parallel fractures or an orthorhombic media. It has an approximate area of $57 \times 57$cm$^2$ and a thickness of $7$cm (Figure 7).

## EXPERIMENTAL PHENOLIC LAYER

### Group velocity measurements

We acquired 3C transmission seismic data over the physical phenolic model described previously, which is intended to simulate a medium with parallel vertical fractures. The vertical, radial, and transverse component data were all acquired, utilizing P-transducers, radially polarized S-transducers, and transversely polarized S-transducers, as source and receivers, respectively. For each component, the source and receiver transducers always had identical polarizations. The P- and S-transducers are Panametric $V103$ and $V153$ with diameters of $13$ mm and a scaled nominal central frequency of $32$Hz for P-wave. For the acquisition, the reference Cartesian coordinate system was chosen to be the same as the orthorhombic symmetry system. As the symmetry of phenolic materials is relatively well controlled, the Cartesian axes were aligned with the symmetry planes of the phenolic layer. The transmission receiver lines were positioned along $0^\circ$, $90^\circ$, $45^\circ$, and $135^\circ$ azimuths on the model's top surface (Figure 8a-d), with the source located at the bottom; and $0^\circ$, $90^\circ$ azimuth receiver lines on the top surface were used with the source also on the top of the model, offset some distance from the receiver line (Figure 8e-f). The group velocities along different directions in the $(x_1, x_3)$, $(x_2, x_3)$, azimuth $45^\circ$, and azimuth $135^\circ$ planes were estimated from the transmission profiles in Figure 8a-d. The group velocities along different directions in the $(x_1, x_2)$ plane were estimated from the profiles in Figure 8e-f.

Figure 10 shows the 3C data from one of our transmission shot gathers. The shear-wave splitting phenomenon is observed between the radial and transverse components (Figure 10c-d), with the zero-offset arrivals of the qS-waves at different arrival times (approximately $0.45$ms and $0.41$ms, respectively). The qP group velocities are determined

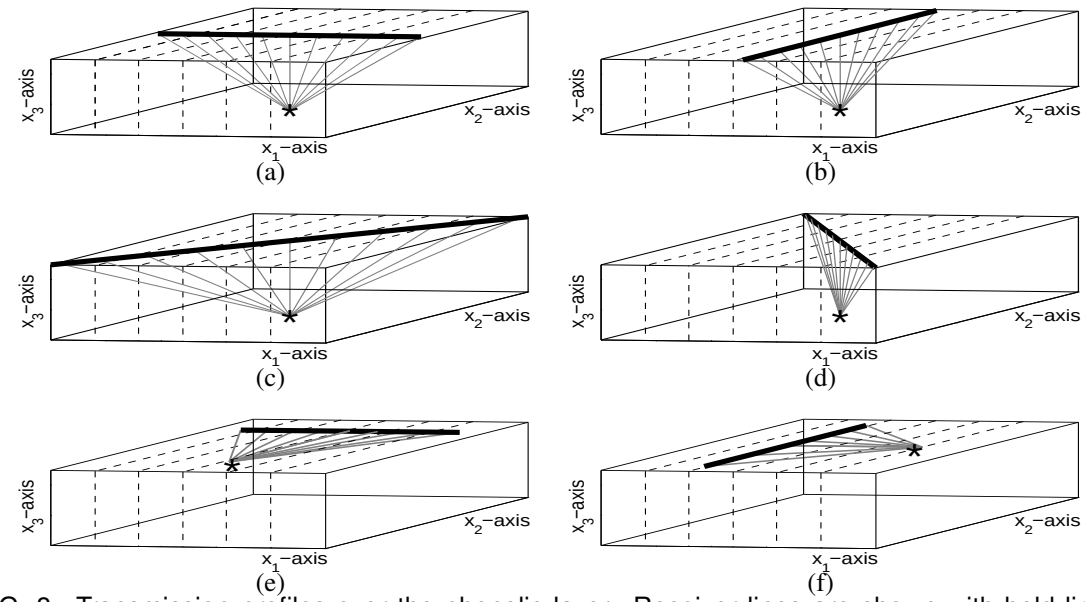


FIG. 8. Transmission profiles over the phenolic layer. Receiver lines are shown with bold lines, sources by $\star$, the raypaths connecting source-receivers with thin lines and slab joints with dash lines. Receiver lines at top surface along $0^\circ$, $90^\circ$, $45^\circ$, and $135^\circ$ with respect to $x_1$-axis are shown in panels (a-d). The source is located at the bottom surface. Receiver lines on the top surface along angular directions of $0^\circ$, and $90^\circ$ with the source also located on the top surface are shown in panels (e-f).

from qP first arrival traveltimes picked on the vertical component data. The qS$_V$ and qS$_H$ group velocities are obtained from the qS-wave first arrivals picked on the radial and transverse data components. The qP and qS$_H$ first arrivals are strong and easy to pick. The qS$_V$ first arrivals, however, are more difficult to identify and pick (Figure 10b) from raw radial component data. The horizontal component of the reflected qP-wave first arrival event appears rather strong in the radial-component data, and because of its velocity (almost twice that of the shear waves) greatly interferes with the first arrivals of the qS$_V$-wave, making the picking of the direct arrival of the qS$_V$-wave difficult, especially for the middle-angle range. To overcome this difficulty, radial trace filtering (Henley, 2003) was applied to the radial component data. This estimate-and-subtract method attenuates the interference from events whose local dip differs from that of the qS$_V$ first arrival event. Done carefully, this type of radial filtering does not introduce traveltime changes to the target event (static shift) and also preserves the amplitude (Henley, 2003).

The qP and qS velocities along the $x_1$-, $x_2$-, and $x_3$-axes are listed in Table 2. We estimated the errors as $\pm 70$m/s and $\pm 35$m/s for the qP- and qS-velocities measured from physical model data, using 1m error in distance (scaled), $0.004$s error for qP-wave first arrival time picks ($1/8$ of the dominant wavelength of the 32Hz wavelet), and $0.007$s error for qS-waves first arrival time picks ($1/8$ of the dominant wavelength of the 17Hz wavelet). The qP and qS group velocity surfaces for the symmetry planes, polar plots of group velocity versus group angle are shown in Figure 9. The qS$_H$ wavefronts are purely ellipsoidal. The qP wavefronts deviate slightly from the ellipsoidal (shown by gray curves) with smaller velocities (at middle-angle range) compared to the ellipse. The qS$_V$ wavefronts also deviate from the spherical with slightly larger velocities (at middle-angles range) compared to the circle (grey curve).

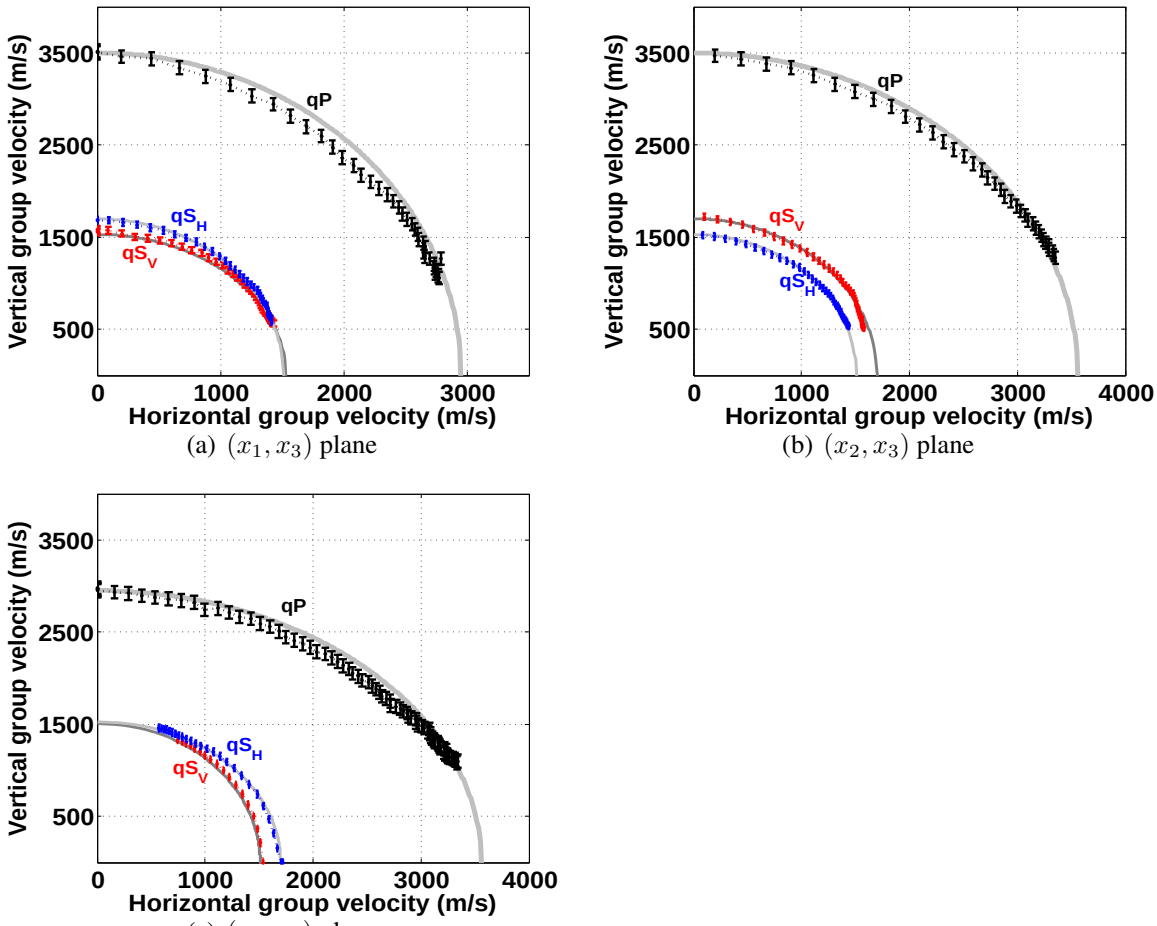


(a) $(x_1, x_3)$ plane

(b) $(x_2, x_3)$ plane

(c) $(x_1, x_2)$ plane

FIG. 9. The group velocity surfaces for the three modes (qP, qS$_V$, qS$_H$) in the three symmetry planes. An elliptical wavefront is plotted for comparison in solid grey. The measured velocities in the $0^\circ$ and $90^\circ$ directions are considered to be the major and minor axes of the ellipse. Group angles are plotted with respect to the vertical axis for the $(x_1, x_3)$ and $(x_2, x_3)$ planes, and with the $x_1$-axis for the $(x_1, x_2)$ plane.

| $V_{11}$ | $V_{22}$ | $V_{33}$ | $V_{23}$ | $V_{13}$ | $V_{12}$ |
|---|---|---|---|---|---|
| $2950 \pm 70$ | $3640 \pm 70$ | $3500 \pm 70$ | $1700 \pm 35$ | $1530 \pm 35$ | $1510 \pm 35$ |

Table 2. Phenolic qP- and qS-velocity (m/s) in principal directions. Here $V_{ij}$ $(i, j = 1, 2, 3)$ is the body wave velocity which propagates along the $x_j$-axis and is polarized along the $x_i$-axis. For example $V_{11}$ is the qP-wave velocity propagating along the $x_1$-axis, and $V_{23}(= V_{32})$ is the qS-wave velocity propagating along the $x_3$-axis and polarized along the $x_2$-axis.

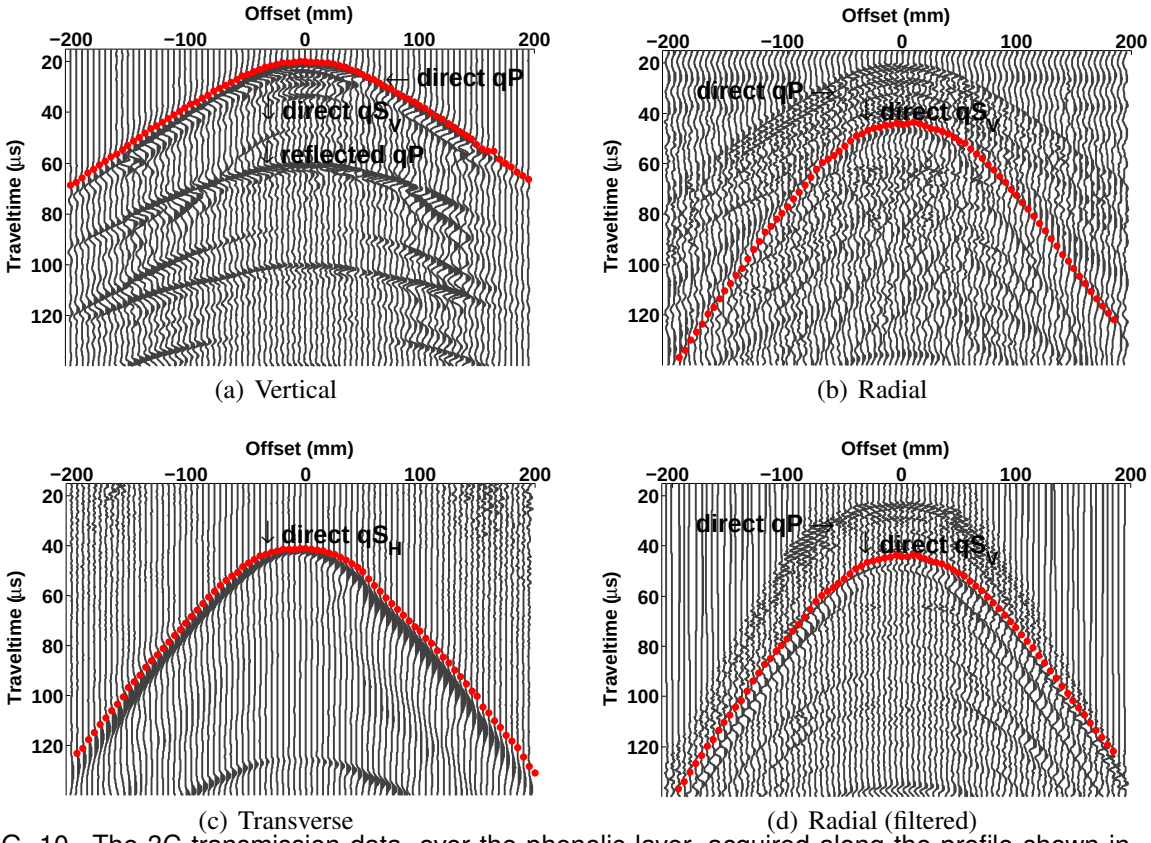


(a) Vertical (b) Radial

(c) Transverse (d) Radial (filtered)

FIG. 10. The 3C transmission data, over the phenolic layer, acquired along the profile shown in Figure 8a, with the wave propagation at the $(x_1, x_3)$-plane. (a) Raw vertical-component data. (b) Raw radial-component data. (c) Raw transverse-component data. (d) Filtered radial-component data (radial trace filtering). Red dots are first arrival picks of each mode. Displayed data have a long-gate automatic gain control applied for the vertical and transverse components. The radial component data have been displayed with a shorter window automatic gain control to boost the direct qS$_V$ arrival. The three components have similar noise levels.

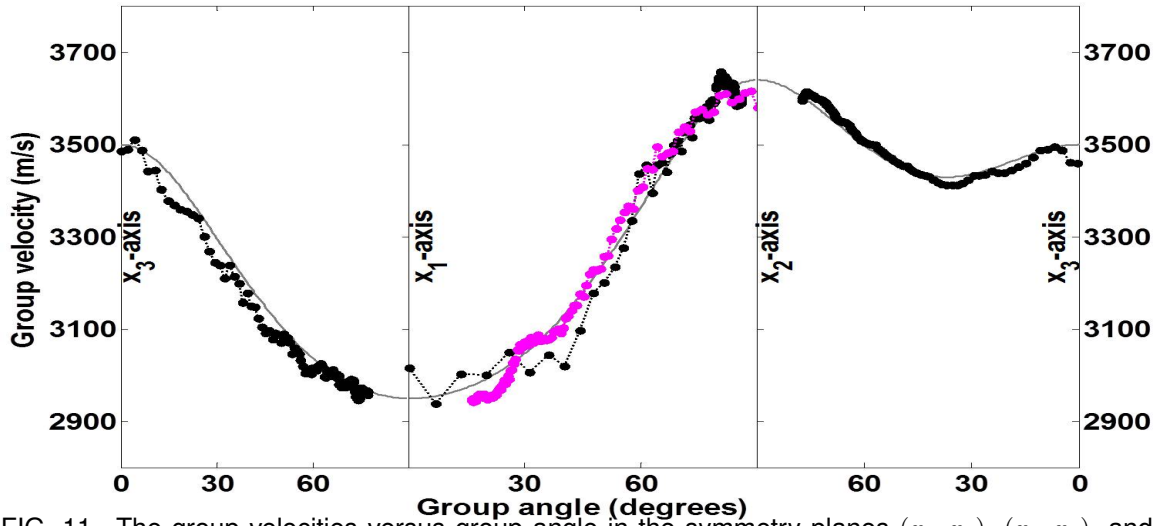


FIG. 11. The group velocities versus group angle in the symmetry planes $(x_1, x_3)$, $(x_2, x_3)$, and $(x_1, x_2)$. The solid gray lines are velocities calculated from estimated parameters and the dotted lines are measured ones. In $(x_1, x_2)$ plane the black dotted line measured from a receiver profile along $x_2$-axis, the magenta dotted line measured from a receiver profile along $x_1$-axis.

The group velocity measurements from transmission data collected by $13$mm transducers, which are the commonly used transducers in physical modeling on solid surfaces, are used to estimate the experimental phenolic layer stiffness coefficients presented in Mahmoudian et al. (2013). Figure 11 compares the measured qP group velocities from transmission data collected by $1.1$mm transducers and group velocities calculated from the estimated $A_{ij}$; the calculated velocities match the measured velocities reasonably well.

Some small discrepancies between the theoretical group velocities and measured group velocities could be due to our assumption of homogeneity for the simulated fractured layer or the employment of the approximate orthorhombic group velocity expression rather than an exact form. The measured phase velocities are also compared to the theoretical velocities predicted from the estimated $A_{ij}$ (Figure 12). Good agreement within the error range of velocity measurements is obtained.

## Phase Velocity Measurements

For each symmetry plane, we acquired two transmission seismic data gathers with the source at two different depths from the receiver plane. The P-transducers (piezoelectric pin CA-1135) with each piezoelectric element being $1.1$mm in diameter were used to produce the vertical component data. Using the method discussed in Kebaili and Schmitt (1997), we measured the phase velocity for the three symmetry planes. We took great care picking on the $(\tau, p)$ transforms, a small window AGC (automatic gain control) used in order to enable consistent picking on first arrivals.

The measured phase velocities are also compared to the theoretical velocities predicted from the estimated $A_{ij}$ (Figure 12). Good agreement within the error range of velocity measurements is obtained. This indicates that the estimated $A_{ij}$ from group velocity measurements can be used to obtain the phase velocities with high accuracy.

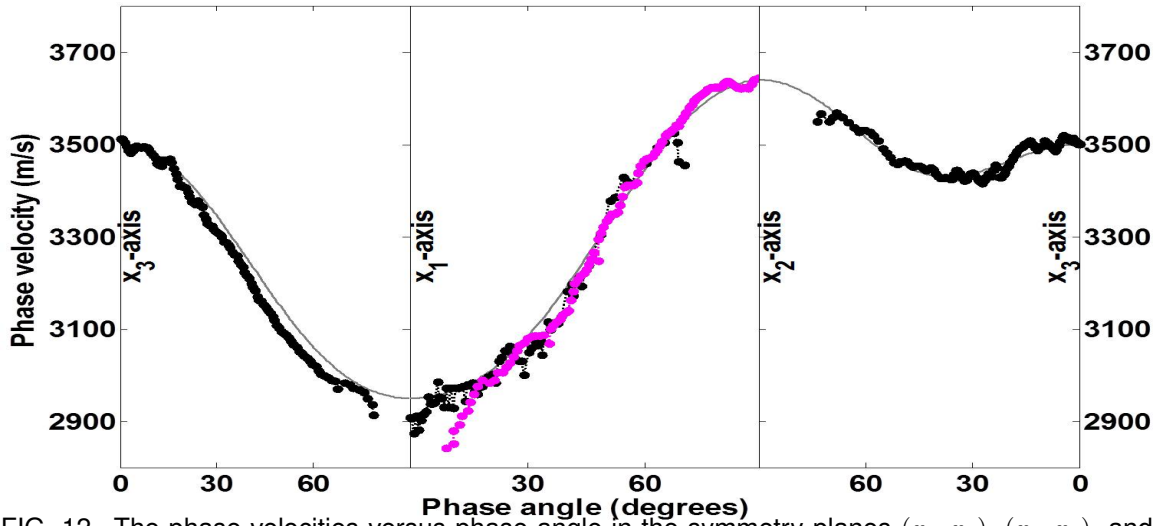


FIG. 12. The phase velocities versus phase angle in the symmetry planes $(x_1, x_3)$, $(x_2, x_3)$, and $(x_1, x_2)$. The solid gray lines are theoretical velocities and the dotted lines are measured ones. In $(x_1, x_2)$ plane the black dotted line was measured from a receiver profile along $x_2$-axis, the light grey triangle line was measured from a receiver profile along $x_1$-axis.

## SUMMARY AND CONCLUSIONS

We obtained the group velocities in various directions through a phenolic medium with orthorhombic anisotropy. This was done by recording 3C ultrasonic transmission seismograms with 13mm diameter piezoelectric transducers as sources and receivers, picking direct arrival traveltimes, and dividing these by source-receiver nearest-edge distances. To account for large transducer diameters, we used edge-to-edge distances rather than center-to-center distances. The effective diameters of transducers were carefully determined from velocity measurements made over a known isotropic material in advance of any anisotropic experiment. Using edge-to-edge correction, the qP traveltime measurements with 13mm-diameter transducers, picked on vertical component data, were consistent with the ones made with smaller (1.1mm- and 6mm-diameter) transducers. Using very small point transducers, the measurements of group velocities obviously will not need an extra edge-to-edge correction. However, very small transducers do not usually produce a powerful enough signal for large physical models, and they have coupling issues, experimental challenges which we should be able to manage in the near future. The qS$_V$-wave from 13mm transducers, was difficult to identify and pick on radial component data, and radial trace filtering was used to help with the picking.

An alternative method commonly used for estimating $A_{ij}$ is based on the well-known exact relationship between phase velocity within the symmetry planes and the stiffness coefficients. The phase velocities for waves from an impulsive source can be determined by applying the $(\tau, p)$ transform to the transmission gathers with the sources at two different depths. Since the $(\tau, p)$ transform method is dependent on identifying and picking the times of unique wavefronts, the closer the transducers are to approximating point sources and point receivers, the better suited the data will be for this derivation. Large transducers appear not to be suitable for this application, because the wavefronts associated with large transducers are superpositions of energy pulses from different parts of the active faces of the transducers. Picking consistently on the strong peak or trough of the transformed wavefront

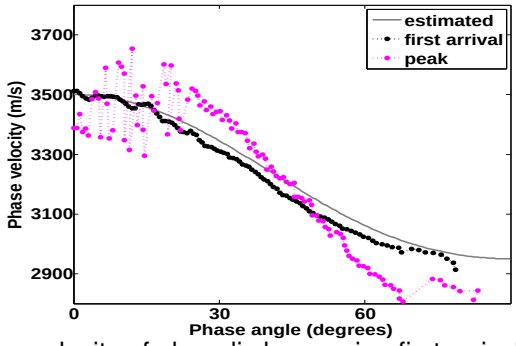


FIG. 13. Measured qP phase velocity of phenolic layer using first arrival picks compared to picking on strong peak, from transmission data collected by 1.1mm transducers. The propagation plane is the $(x_1, x_3)$ plane.

will result in different trends for the phase velocities (Figure 13). Estimation of $A_{ij}$ from phase velocities, because of the exact formula, are potentially more accurate. However, the limitations imposed on the measurements of the phase velocities in the laboratory give the group method a definite advantage on real data.

Theoretical phase and group velocities calculated using values of $A_{ij}$ estimated from experimental group velocities agreed with the experimental phase and group velocities, respectively, validating the $A_{ij}$ estimates. Our phenolic experimental layer, now with known elastic properties, is intended to be used in a modeling study for traveltime and quantitative amplitude analysis of fractured media.

We assume homogeneity in our simulated fractured medium. The very slight frequency dispersion observed in the data (wavelet shapes broaden in time as source-receiver offsets increase) is likely mostly due to the wave interference caused by the large size transducers. We have demonstrated this pulse broadening numerically by finite-difference modeling of the response of an extended source shooting into an extended receiver through a non-dispersive medium (note the pulse broadening in Figure 2a). The simulation shows a stretching of the wavelet from near to far offset. Therefore, the wavelet shape change observed in physical model data should be mostly due to the dimensions of the source and receiver, and is not likely due to an intrinsic frequency dispersion effect.

## ACKNOWLEDGMENTS

The industrial sponsors of the Consortium for Research in Elastic Wave Exploration Seismology (CREWES) and the National Science and Engineering Research Council of Canada (NSERC) provided financial support for this research. Dave Henley is acknowledged for the application of radial trace filtering on the radial component data.

## REFERENCES

Bouzidi, Y., and Schmitt, D. R., 2009, Measurement of the speed and attenuation of the Biot slow wave using a large ultrasonic transmitter: Journal of Geophysical Research, **114**, No. B08.

Brown, R. J., Lawton, D. C., and Cheadle, S. P., 1991, Scaled physical modeling of

anisotropic wave propagation: multioffset profiles over an orthorhombic medium: Geophysical Journal International, **107**, No. 3, 693–702.

Dellinger, J., and Vernik, L., 1994, Do traveltimes in pulse-transmission experiments yield anisotropic group or phase velocities?: Geophysics, **59**, No. 11, 1774–1779.

Ebrom, D. A., and McDonald, J. A., 1994, Seismic physical modeling: Geophysics Reprint Series: Society of Exploration Geophysicists, Tulsa, OK.

Henley, D. C., 2003, Coherent noise attenuation in the radial trace domain: Geophysics, **68**, No. 4, 1408–1416.

Kebaili, A., and Schmitt, D. R., 1997, Ultrasonic anisotropic phase velocity determination with radon transformation: Journal of the Acoustical Society of America, **101**, 3278–3286.

Mah, M., and Schmitt, D. R., 2001, Experimental determination of the elastic coefficients of an orthorhombic material: Geophysics, **66**, No. 4, 1217–1225.

Mahmoudian, F., Margrave, G. F., Daley, P. F., Wong, J., and Henley, D., 2013, Estimation of anisotropic elastic stiffness coefficients of an orthorhombic physical model using group velocity analysis on transmission data: Accepted for publication in the Geophysics.

McSkimin, H. J., 1967, Physical acoustics, vol. I, Part A: Academic NewYork.

Musgrave, M. J. P., 1970, Crystal Acoustics: Holden-Day, San Francisco.

Tsvankin, I., 1997, Anisotropic parameters and P-wave velocity for orthorhombic media: Geophysics, **62**, No. 4, 1292–1309.

Vestrum, R. W., 1994, Group- and phase-velocity inversions for the general anisotropic stiffness tensor: University of Calgary, M.Sc. Thesis.

Vestrum, R. W., Lawton, D. C., and Schmitt, R., 1999, Imaging structures below dipping TI media: Geophysics, **64**, No. 4, 1239–1246.

Wong, J., Hall, K. W., Gallant, E. V., Maier, R., Bertram, M., and Lawton, D. C., 2009, Seismic physical modeling at University of Calgary: Canadian Society of Exploration Geophysicists Recorder.